Neurochemistry International 129 (2019) 104485

Contents lists available at ScienceDirect

Neurochemistry International

journal homepage: www.elsevier.com/locate/neuint

Phospho-mTOR expression in human glioblastoma microglia-macrophage cells

Lucia Lisi[a,*], Gabriella Maria Pia Ciotti[a], Marta Chiavari[a], Michela Pizzoferrato[a], Annunziato Mangiola[b], Sergey Kalinin[c], Douglas L. Feinstein[c,d], Pierluigi Navarra[a,e]

[a] Institute of Farmacologia, Università Cattolica del Sacro Cuore, L.go F. Vito 1, Rome, Italy
[b] Department of Neuroscience, Imaging and Clinical Sciences, Università degli Studi G. D'Annunzio Chieti-Pescara, via Colle dell'Ara 100, Chieti, Italy
[c] Department of Anesthesiology, University of Illinois at Chicago, Chicago, IL, USA
[d] Department of Veterans Affairs, Jesse Brown VA Medical Center, Chicago, IL, USA
[e] Fondazione Policlinico Universitario Agostino Gemelli, L.go F. Vito 1, Rome, Italy

ARTICLE INFO

Keywords:
Glioblastoma
Microglia
mTOR
TSC2
Tumor microenvironment
Molecularly targeted therapies

ABSTRACT

The glioblastoma (GBM) immune microenvironment is highly heterogeneous, and microglia may represent 30–70% of the entire tumor. However, the role of microglia and other specific immune populations is poorly characterized. Activation of mTOR signaling occurs in numerous human cancers and has roles in microglia-glioma cell interactions. We now show in human tumor specimens (42 patients), that 39% of tumor-associated microglial (TAM) cells express mTOR phosphorylated at Ser-2448; and similar mTOR activation is observed using a human microglia-glioma interaction paradigm. In addition, we confirm previous studies that microglia express urea and ARG1 (taken as M2 marker) in the presence of glioma cells, and this phenotype is down-regulated in the presence of a mTOR inhibitor. These results suggest that mTOR suppression in GBM patients might induce a reduction of the M2 phenotype expression in up to 40% of all TAMs. Since the M2 profile of microglial activation is believed to be associated with tumor progression, reductions in that phenotype may represent an additional anti-tumor mechanism of action of mTOR inhibitors, along with direct anti-proliferative activities.

1. Introduction

Glioblastoma (GBM - grade IV glioma) is the most aggressive primary brain tumor, characterized by a high rate of therapeutic failures despite aggressive treatments, and a poor prognosis. Tumor classification is based on malignancy, nuclear atypical and infiltration of the surrounding brain parenchyma. Unfortunately, the tumor is often diagnosed once the patients become symptomatic, at which time the lesion is already widely extended. The gold standard of therapy, established over a decade ago, consists of fractionated radiotherapy in combination with classical chemotherapy with temozolomide; however, in almost all cases, chemotherapeutic resistance arises and recurrence is common after initial therapy (Weller, 2018; Lu et al., 2018).

The clinical success of cancer immunotherapies targeting T-cell immune checkpoint receptors PD-1/PD-L1 has demonstrated the importance of immune-evasion as a hallmark of cancer. On the side of innate immune responses, the recent preclinical and clinical development of novel CCR2 antagonists to control the trafficking of macrophage-monocyte lineage belongs to the same conceptual framework (Liang et al., 2018; Amin et al., 2018; Tsutsumi-Kuroda et al., 2018). These immunotherapeutic drugs include antibody-drug conjugates, peptide vaccines, autologous infusions of modified chimeric antigen receptor-expressing T cells, autologous dendritic cell vaccines, oncolytic viruses, immune-stimulatory viruses, checkpoint blockade inhibitors, and drugs acting on innate immune cells (Miyauchi and Tsirka, 2018).

The GBM immune microenvironment is heterogeneous and can differ in GBM subtypes (Chen and Hambardzumyan, 2018). Although manipulation of the tumor microenvironment was shown to be able to repress GBM tumor progression (Arbab et al., 2017), the role of specific immune populations remains poorly characterized. Microglia are the principal resident immune cells in the central nervous system (CNS) and are thought to be versatile players in both inflammatory and physiological contexts. Although the past decade has seen important progress in the understanding of multi-tasking microglia in GBM pathology, the relative importance of microglia at different disease stages and how

* Corresponding author. Institute of Pharmacology, Università Cattolica Del Sacro Cuore, L.go F. Vito 1, 00168, Rome, Italy.
E-mail address: lucia.lisi@unicatt.it (L. Lisi).

https://doi.org/10.1016/j.neuint.2019.104485
Received 23 January 2019; Received in revised form 1 May 2019; Accepted 3 June 2019
Available online 10 June 2019

microglia could be targeted for optimal therapeutic efficacy remain largely enigmatic. Glioma associated microglia (GAMs) constitute the largest portion of tumor infiltrating cells, contributing between 30 and 70% to the glioma mass (Wood and Morantz, 1979; Roggendorf et al., 1996; da Fonseca and Badie, 2013). Different profiles of activation coexist in the same tumor, depending on GAM location or stage of disease (Dello Russo et al., 2017). In particular, GAMs are exposed to factors inducing them to produce cytokines and chemokines, which contribute to tumor growth and to maintain a pro-tumorigenic, immunosuppressed microenvironment. Therefore, a bi-directional interaction exists between microglia and GBM. In this context, we previously investigated the *in vitro* interactions between rat microglia and C6 glioma cells (Lisi et al., 2014a). Exposure to conditioned media obtained from C6 cells taken under baseline conditions induced a predominant M2-like phenotype in the microglia. Conversely, if C6 cells were exposed to a medium containing pro-inflammatory stimuli, the subsequent exposure of microglia to such medium was followed by a shift towards an M1-like phenotype (Lisi et al., 2014a). In addition, we investigated the status of microglia/macrophage activation in surgical specimens from 41 patients diagnosed with grade IV GBM. For each patient we analyzed both the center of the tumor and the surrounding parenchyma. Four different markers, namely IBA-1, CD163, iNOS and ARG-I were investigated and we showed that M2 markers (in particular CD163) rather than M1 markers could be envisioned as a prognostic marker (Lisi et al., 2017a).

The phospho-inositide 3 kinase (PI3K)/protein kinase B (AKT)/mammalian target of rapamycin (mTOR) pathway is a well-investigated signaling pathway that regulates diverse cellular functions including proliferation, metabolism and transcription (Tee, 2018). Activation of mTORC1 is observed in numerous human cancers due to gain-of-function mutations in oncogenes (PI3K, AKT or Ras) and/or loss-of-function mutations in tumor suppressors (PTEN, LKB1, or TSC1/2) (Foster and Fingar, 2010). In addition, a direct role of mTOR in the modulation of glial functions has been described. Data from ourselves and other groups support the notion that mTOR is involved in glial pro-inflammatory activation (Dello Russo et al., 2009; Lisi et al., 2011) and in microglia-glioma interactions (Lisi et al., 2014b). In an *in vitro* rat model, we showed that the inhibition of mTOR polarizes glioma-activated microglial cells towards the M1 phenotype, and in parallel prevents the induction of the M2 status that promotes tumor growth (Lisi et al., 2014b). Although the relevance of mTOR in glioma biology is now well established, initial studies with mTORC1 inhibitors, such as rapamycin (RAPA) and its analogs, showed limited efficacy in clinical trials (Martelli et al., 2018). Despite such initial failures, newer mTOR inhibitors are being investigated; ClinicalTrials.gov currently lists 478 ongoing studies on mTOR and cancer, 28 out of them being focused on glioma. Most of these trials are testing ATP-competitive mTOR inhibitors, alone or in combination with monoclonal antibodies; this strategy targets both GBM cells and GAM functions, thereby raising the need for further research into this area.

In the present work, we adopted two different approaches, i.e. human tumor specimens and human cell models, to characterize the activation of the mTOR pathway in GAMs. In particular, using immunostaining analysis of surgical GBM specimens obtained from 42 patients, we evaluated phosphorylated-mTOR expression and localization to microglial cells and using three human cell lines, we investigated the involvement of mTOR in an *in vitro* microglia-glioma interaction paradigm.

2. Methods

2.1. Materials

Cell culture reagents [Dulbecco's modified Eagle's medium (DMEM), DMEM-F12 and Fetal calf serum (FCS)] were from Invitrogen Corporation (Paisley, Scotland). Antibiotics were from Biochrom AG (Berlin, Germany). Bacterial endotoxin LPS (*Salmonella typhimurium*) was from Sigma–Aldrich (St. Louis, MO, USA). The rat recombinant interferon-γ (IFNγ) was purchased from Endogen (Pierce Biotechnology, Rockford, IL, USA). The human recombinant interleukin 1β (IL1β), human IFNγ and recombinant human Tumor necrosis factorα (TNFα) were purchased from R&D System. β-actin (clone AC-74) mouse monoclonal antibody was from Sigma Aldrich; rabbit polyclonal anti-phospho [ser-2448] mTOR and rabbit polyclonal anti-total mTOR were purchased from Novus Biological (Littleton, CO, USA); mouse monoclonal p70 S6 was purchased from Santa Cruz Biotechnology; rabbit polyclonal 4EBP1 was purchased from Bethyl Laboratories; monoclonal rabbit Tuberin/TSc2 was purchased from Cell Signaling Technology, goat monoclonal AIF-1/Iba1 was purchased from Novus Biological. Arginase I (E−2) mouse monoclonal antibody was purchased from Santa Cruz Biotechnology.

2.2. Cell cultures

The human microglia cell line (CHME-5; RRID:CVCL_5J53) was kindly provided by professor Pierre Talbot (Janabi et al., 1995). Human U87MG and T98G glioma cell lines were kindly provided by professor Grazia Graziani (Tor Vergata University- Rome). CHME-5, U87MG and T98G cells were grown in DMEM containing 10% FCS and antibiotics and studies carried out at a low concentration of FCS (1%). Cells were passed twice a week and plated for experiments at 2×10^4 cells/well. All the experiments received institutional approval.

Conditioned media from activated glioma cells was generated following a protocol which removed the proinflammatory stimulus from the medium. Briefly, in preliminary experiments glioma cells were incubated in the presence of mixture of cytokines (10 ng/ml TNFα, 10 ng/ml IL1β, 10 UI/ml hIFNγ (TII) for 4, 8 or 24 h (Fig. 3). Proinflammatory mRNA levels were evaluated by real time quantitative PCR (qPCR). Based on the results, the glioma-CM were prepared as follows:

A) B-CM: 4 h incubation in plain medium, followed by 3 washes with phosphate buffered saline (PBS) and addition of fresh plain medium for 24 h. After this second period of incubation, the CM was collected, centrifuged to remove cellular debris and stored as B-CM.
B) PS-CM: 4 h incubation with TII, followed by 3 washes with PBS and addition of fresh plain medium for 24 h. After this second period of incubation, the CM was collected, centrifuged and stored as PS-CM.

Both CM were stored at −80 °C until the experiments on CHME-5 cells were performed.

A flow chart of the studies shows the experimental design (Scheme 1).

2.3. Viability assay

The cell viability was measured using a specific luminescence kit: CellTiter-Glo® Luminescent Cell Viability Assay (Promega). Cell mortality was detected using a specific fluorescence kit: RealTime-Glo™ MT Cell Viability Assay (Promega). The assays were carried out according to the manufacturer's instructions.

2.4. Nitrite assay

iNOS activity was assessed indirectly by measuring nitrite accumulation in the incubation media. Briefly, an aliquot of the cell culture media (80 µL) was mixed with 40 µL Griess Reagent (Sigma-Aldrich) and the absorbance measured at 550 nm in a spectrophotometric microplate reader (PerkinElmer Inc., MA, USA). A standard curve was generated during each assay in the range of concentrations 0–100 µM using $NaNO_2$ (Sigma-Aldrich). In this range, the assay was linear and the minimum detectable concentration of NaNO2 was ≥3.12 µM. The protein content in each sample was determined by Bradford's method

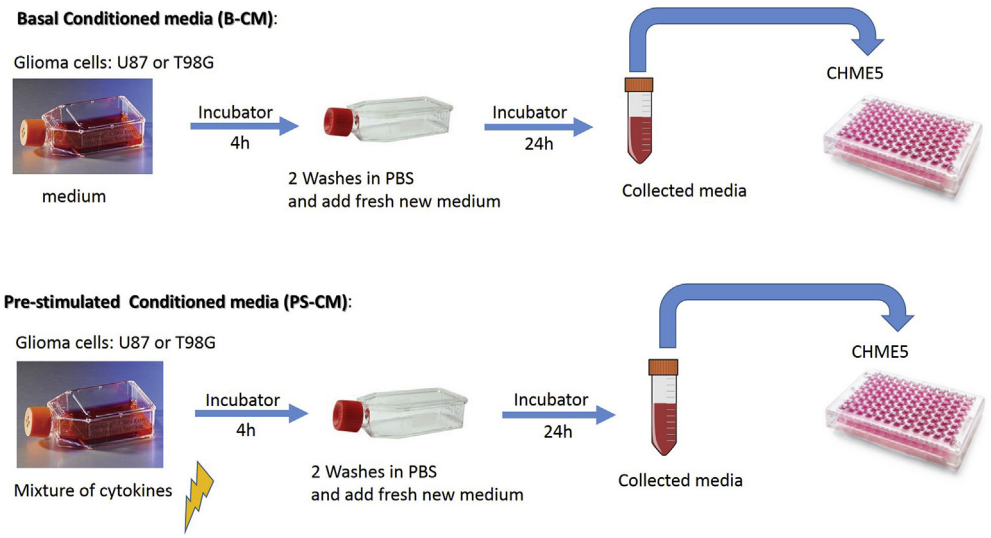

Scheme 1. Metodological flow chart of the study.

(Biorad, Hercules, CA, USA) using bovine serum albumin as standard.

2.5. Urea assay

Urea levels in CHME-5 cells were detected by the QuantiChrom Urea Assay kit (BIOassay System, Hayward, CA, USA), used according to the manufacturer's instructions. Briefly after 48 h of incubation with the test substances, an aliquot of cell culture media (50 µl) was mixed with 200 µL Urea Reagent (Bioassay system) and the absorbance measured at 430 nm in a spectrophotometric microplate reader (PerkinElmer Inc., MA, USA). A standard curve was generated during each assay in the range of concentrations 0–100 µg/ml using Urea as standard. In this range, standard detection was linear and the minimum detectable concentration of Urea was 3.12 µg/ml. The protein content in each sample was determined by Bradford's method (Biorad, Hercules, CA, USA) using bovine serum albumin as standard.

2.6. mRNA analysis in real time PCR

Total cytoplasmic RNA was extracted using the RNeasy Micro kit (Qiagen, Hilden, Germany), which included 15 min DNase treatment. RNA concentration was measured using the Qubit™ RNA HS Assay Kit (Thermo Fisher Scientific). Aliquots (0.5 µg) of RNA were converted to cDNA using random hexamer primers. Quantitative changes in mRNA levels were estimated by real time PCR using the following cycling conditions: 35 cycles of denaturation at 95 °C for 20 s; annealing and extension at 60 °C for 20 s; using the Brilliant III Ultra-Fast SYBR® Green QPCR Master Mix (Stratagene, La Jolla, CA, USA). PCR reactions were carried out in a 20-µL reaction volume in Ariamx real time PCR machine (Stratagene). Primers used for the evaluation of gene expression are reported in Table 1. Relative mRNA concentrations were calculated from the take-off point of reactions (threshold cycle, Ct) using the comparative quantitation method provided by Stratagene software and based upon the -ΔΔCt method. This analysis approximates a given sample's target mRNA (e.g. IL6) level relative to the mean of the target mRNA levels in untreated controls ("calibrator" value), thus permitting statistical analysis of deviation from the mean even among the controls. Ct values for α-tubulin expression served as a normalizing signal. In each assay, the PCR efficiency was also calculated using serial dilution of one experimental sample; efficiency values between 94 and 98% were found for each primer set and taken into account for the comparative quantitation analysis (Dello Russo et al., 2009).

2.7. IL1β, IL6 and PGE2 quantification

IL1β, IL6 and PGE2 levels in the incubation medium were detected using a specific Enzyme Immunoassay kit (EIA) for PGE2 (ELABscience), and a specific enzyme-linked immunosorbent assay (ELISA) for IL1β and IL6 (R&D System). The assays were carried out according to the manufacturer's instructions.

2.8. Western immunoblot

The cells were lysed in RIPA buffer (1 mM EDTA, 150 mM NaCl, 1% igepal, 0.1% sodium dodecyl sulfate, SDS, 0.5% sodium deoxycholate, 50 mM Tris–HCl, pH 8.0) (Sigma-Aldrich) containing protease inhibitor cocktail diluted 1:250 (Sigma–Aldrich). The protein content in each sample was determined by Bradford's method (Biorad, Hercules, CA,

Table 1
Primers used for the evaluation of gene expression.

Genes	Forward	Reverse	Product length
ARG1	TTCTCAAAGGGACAGCCACG	AGCACCAGGCTGATTCTTCC	272
ARG2	ACCTCAGAGGAAGAGGCGAA	AAATGTCCCCATTAAGGCAGT	276
COX2	TG CTG GCA GGG TTG CTGGTGGTA	CAT CTG CCT GCT CTG GTC AAT CGA A	86
IL10	GGCACCCAGTCTGAGAACAG	CGCCTTGATGTCTGGGTCTT	255
IL1β	AGC CAT GGC AGA AGT ACC GT	TCC ATG GCC ACA ACA ACT GA	219
IL6	GGC TCA TTC TGC CCT CGA GCC	GGA CCG AAG GCG CTT GTG GAG	100
iNOS	CTGCATGGAACAGTATAAGGCAAA C	CAGACAGTTTCTGGTCGATGTCATGA	230
Raptor	GGT GCT GTT AAG CCA AGT GC	TGT TCA GCT GGC ATG TAG GG	279
Rictor	TGG GCG AGG TTT CCG GT	GTC ATT CCG CCC TCG TAC TC	99
TGFβ	CATG GAG CTG GTG AAA CGG A	CGG GTG ACT TCT TTG GCG TA	219
Tubuline	CCC TCG CCA TGG TAA ATA CAT	ACT GGA TGG TAC GCT TGG TCT	110

USA) using bovine serum albumin as standard. A 100 μg aliquot of protein was mixed 1:2 with 2X Laemmli Buffer (Biorad), boiled for 5 min, and separated through 10% polyacrylamide SDS gels. Apparent molecular weights were estimated by comparison to colored molecular weight markers (Sigma Aldrich). After electrophoresis, proteins were transferred to polyvinylidene difluoride membranes by semi-dry electrophoretic transfer (Biorad). The membranes were blocked with 10% (w/v) low-fat milk in TBST (10 mMTris, 150 mMNaCl, 0.1% Tween-20, pH 7.6) (Biorad) for 1 h at room temperature, and incubated in the presence of the primary antibody overnight with gentle shaking at 4 °C. Primary antibodies for rabbit Polyclonal anti-phospho mTOR (NB600-607-novus), rabbit polyclonal anti-mTOR (NB-novus), mouse monoclonal anti β-actin clone AC-74 (A531-Sigma), mouse monoclonal anti p-p70 S6 kinase α (A-6) (sc-8416-Santa Cruz), rabbit Polyclonal anti-4EBp1 (A300-501A-Bethyl), and rabbit monoclonal anti Tuberin/TSC (D93F12) (4308 – Cell Signaling) were used at the final concentration of 1:1000. Primary antibodies were removed, membranes washed 3 times in TBST, and further incubated for 1 h at room temperature in the presence of specific secondary antibody diluted 1:15,000. Following three washes in TBST, bands were visualized by incubation in ECL reagents (GE Healthcare) and exposure to Hyperfilm ECL (GE Healthcare NY, USA). The same membranes were washed 3 times in TBST, blocked with 10% (w/v) low-fat milk in TBST for 1 h at room temperature and used for β-actin immunoblot.

2.9. Immunostaining

Cover glasses of 13 mm of diameter were coated with Collagen I 0,1 mg/ml or Poli-L-lysine 50ug/ml for 1 h at 37 °C, after that three washes in PBS with calcium and magnesium were needed and used to seed the CHME-5 at 20000 cells per well concentration. After 24 h from the treatment, cells were blocked with PAF at 4% concentration in PBS with calcium and magnesium for 20 min at room temperature. After three washes in PBS with calcium and magnesium, cells were blocked with BSA and incubated in presence of primary antibody. The incubation time was overnight for ARG1 1:50; after three washes in PBS with calcium and magnesium in gentle shaking, cells were incubated with secondary antibody (anti-mouse) for 1 h and mounted with Vectashield with DAPI (Vector Laboratories).

2.10. Patients and specimens

We enrolled 42 adults [mean age 60.51 (34–79), 27 males/15 females], who underwent surgery for primary GBM at the Neurosurgery Department, Fondazione Policlinico Gemelli" (Rome, Italy), from March 2005 to September 2011. Diagnosis of GBM was established on histological examination according to the WHO classification (grade IV) of tumors of the CNS. In all cases a total tumor removal was achieved, allowing us to obtain tissues samples from both the tumor and the surrounding macroscopic normal brain tissue (between 1 cm and 2 cm from the tumor border; larger resections were performed in tumors that grew far from eloquent areas). The demographic characteristics for single patient are reported in Table 2. All patients provided written consent to use their specimens for research and the research proposal was approved by the local ethics Ethical Committee (Lisi et al., 2017a).

2.11. Tissue preparation and immunohistochemistry

Human tumor tissue obtained from surgical resection of patients with grade IV GBM were fixed in 4% paraformaldehyde in 0.1 M phosphate buffer pH 7.6 overnight at 4 °C. Dehydration of tissue was through a series of 80%, 95% ethanol one hour each followed by 100% ethanol overnight. Two 100% xylene washes were done for 1 h each and then 1 h in 60 °C Paraplast Plus (Tyco/Healthcare, Mansfield, MA). After a change of Paraplast Plus, tissue was incubated in a 60 °C vacuum oven for 2 h prior to placing in molds to cool and solidify. Sections, 3–4 μm thick, were cut and collected on the superfrost plus slides (Fisher). The PT Link (Dako) was used to deparaffinize and rehydrate the sections and unmask antigen sites. Slides were immersed in 10 mM citrate buffer, pH 6.0, for 10 min at 97 °C and then cooled and washed in PBS or TBS. Endogenous peroxidase activity was inhibited by incubating the slides with Peroxide Block (ScyTek Laboratories, Utah, USA) for 7 min. At this time, point slides washed with PBs underwent single staining procedures, whereas slides washed with TBS underwent double staining procedures.

2.12. Single-staining

After washing in distilled water and then in PBS, slides were incubated with Avidin/Biotin Blocking System (Spring) and washed 3 times in PBS. Nonspecific binding was blocked by 5 min incubation with the Super Block Solution (ScyTek Laboratories, Utah, USA). Sections were incubated for 30 min at room temperature with rabbit anti-human mTOR polyclonal antibody (Novus Biologicals) 1:100, or over-night at 4 °C with goat anti-human Iba1 polyclonal antibody (Novus Biologicals) 1:250. Sections were washed extensively with PBS and subsequently treated with the Ultra Tek HRP Anti-Polyvalent kit (ScyTek Laboratories). Finally, after 3 washes in PBS, sections were treated with 3,3′-diaminobenzidine (ScyTek Laboratories) as chromogen, contrasted with Hematoxylin and mounted.

2.13. Double-staining

The PT Link (Dako) was used to deparaffinize and rehydrate the sections and unmask antigen sites. Slides were immersed in 10 mM citrate buffer, pH 6.0, for 10 min at 97 °C and then cooled and washed in TBS. Endogenous peroxidase activity was inhibited by incubating the slides with Peroxide Block (ScyTek Laboratories, Utah, USA) for 7 min. After washing in distilled water and then in TBS, nonspecific binding was blocked by 10 min incubation with Background Punisher (Biocare-Medical). Sections were incubated for 30 min at room temperature with Rabbit Anti-Human mTOR polyclonal antibody (Novus Biologicals) 1:100 and over-night at 4 °C with Goat Anti-Human Iba1 polyclonal antibody (Novus Biologicals) 1:250. Sections were washed extensively in TBS and subsequently incubated with the MACH 2 Rabbit HRP-Polymer (Biocare-Medical) for mTOR and with Ultratek HRP kit (ScyTek Laboratories) for Iba1. Finally, after 3 washes in TBS, sections were treated with 3,3′-diaminobenzidine (Biocare-Medical) as chromogen for IBA1 and with Vina Green (Biocare-Medical) as chromogen for p-mTOR and then contrasted with Hematoxylin and mounted.

2.14. Immunostaining analysis

Two examiners who were blinded as to the antibody used evaluated staining of human specimens. Both qualitative and quantitative analyses were carried out. For qualitative analysis the intensity of staining was evaluated. In particular, staining was scored on a scale from 0 to 5 where score 0 indicates no significant staining, score 1 very low staining, score 2 low staining, score 3 significant staining, score 4 strong staining and score 5 very strong staining. For quantitative analysis, the number of phospho-mTOR+, IBA1+, or both phospho-mTOR+ and IBA1+ cells were counted in at least 50 cells total. In particular, two blinded examiners have examined three different areas of the same slides and have counted 50 cells that included the number of positive cells for each antibody, the number of positive cells for both antibodies and the number of negative cells (Atzori et al., 2017). In total, the average of six counts was reported as percentage.

2.15. Statistical analyses

Statistical comparison of the differences between pairs of groups was performed by Student's *t*-test. For multiple comparisons ANOVA

Table 2
Demographic characteristic of GBM patients.

GBM patients	Tumor location	Primary (P) Recurrent (R)	Overall survival (months)	WHO classification	Tumor	Peryphery
1	NA[a]	P	13	IV	-[b]	−/+
2	Temporal	P	19	IV	+++	++
3	Temporal	P	60	IV	+++	+++
4	Frontal	R	NA	IV	+	+
5	Frontal	P	7	IV	−/+	−/+
6	NA	P	NA	IV	-	+
7	Frontal	P	15	IV	+++	+
8	Frontal	P	2	IV	+++	−/+
9	Temporal	P	4	IV	+++	+
10	Occipital	P	33	IV	++	+++
11	Temporal	P	14	IV	-	-
12	NA	P	NA	IV	+	+
13	NA	R	NA	IV	++	++
14	Temporal	P	53	IV	+	-
15	Parietal	P	53	IV	-	−/+
16	NA	P	9	IV	-	−/+
17	Frontal	P	NA	IV	-	−/+
18	Frontal	P	NA	IV	+	+
19	Tempo-Parietal	R	53	IV	+++	+
20	Temporal	P	C	IV	-	+
21	NA	P	NA	IV	+	−/+
22	Temporal	P	NA	IV	−/+	+++
23	Parietal	P	6	IV	+	-
24	NA	P	NA	IV	-	+
25	Temporal	P	NA	IV	++	+
26	NA	R	NA	IV	+++	+
27	Frontal	R	NA	IV	++	+
28	Occipital	P	NA	IV	++	++
29	NA	P	NA	IV	++	+
30	Temporal	P	NA	IV	+	−/+
31	NA	P	NA	IV	+++	+
32	Temporal	P	NA	IV	+	+
33	Temporal	P	6	IV	-	+
34	NA	P	NA	IV	−/+	-
35	Frontal	P	12	IV	−/+	+++
36	Fronto-temporal	P	NA	IV	-	+
37	Occipital	P	8	IV	+++	+
38	Frontal	P	NA	IV	++	++
39	Temporal	P	NA	IV	+++	+
40	NA	P	38	IV	++	+++
41	NA	R	24	IV	+++	++
42	Frontal	P	12	IV	++	++

[a] NA: not available.
[b] The number of positive mTOR cells was counted in a total of 50 cells. mTOR staining was scored as percentage of positively stained cells: -, ≤10%; −/+, 11–25%; +, 26–50%; ++, 51–75%; +++, > 75%.

analysis, followed by Bonferroni's post-test or Sidak's test, was used. Statistical significance was determined at $\alpha = 0.05$ level. Differences were considered statistically significant when $p < 0.05$.

3. Results

3.1. mTOR in human glioma specimens

We enrolled 42 patients diagnosed with GBM IV (Table 2). For each patient, we were able to examine glioma specimens as well as the tissue surrounding the tumor by 1–2 cm (periphery). More than 35% of the cells within the glioma tissue and more than 25% of the peripheral cells showed mTOR activation, indicated by phosphorylation at Ser2448. Although the percent of phospho-mTOR-activated positive cells was higher within the tumor, we found no difference in staining intensity between tumor and peripheral tissues (Fig. 1). In addition, in a subgroup of 15 patients showing a higher percentage of phospho-mTOR + cells (39% on average), we carried out a double staining for phospho-mTOR and IBA1 (Fig. 2), a marker of microglia-macrophage cell type. Within the tumor, about 9% of all cells were phospho-mTOR + microglia-macrophages compared to 4.4% within the tissue surrounding the tumor. Looking at IBA1+ cells, we found that about 22% of cells in the glioma specimens were microglia-macrophages; 39% out of these cells are IBA1+ cells expressing phosphorylated-mTOR. Conversely, in periphery of the tumor, 15% of cells are microglia-macrophages, 21% out of these cells express phospho-mTOR (Fig. 2).

3.2. Characterization of U87MG and T98G glioma cell lines

Two different human glioma cell lines, U87MG and T98G, were used to examine their responses to an inflammatory stimulus. Cells were exposed to a mixture of pro-inflammatory cytokines: 10 ng/ml TNFα, 10 ng/ml IL1β, 10 UI/ml IFNγ (TII), after which gene expression was evaluated at different time points (4, 8 and 24 h). IL1β, IL6 and COX2 was significantly increased by TII, with maximal levels at 8 h after which expression decreased (Fig. 3). In contrast, TGFβ and ARG2 expression was not affected by pro-inflammatory stimuli. Neither iNOS, IL10 nor ARG1 mRNAs were detectable either before or after pro-inflammatory stimulation (data not shown).

Based on these results as well as previous data (Lisi et al., 2014a), we prepared glioma conditioned medium (CM) by pre-incubating glioma cells for 4 h with TII or plain medium as control. After pre-incubation, cells were carefully washed and incubated for a further 24 h in plain medium only to generate basal-conditioned medium (B-CM) or

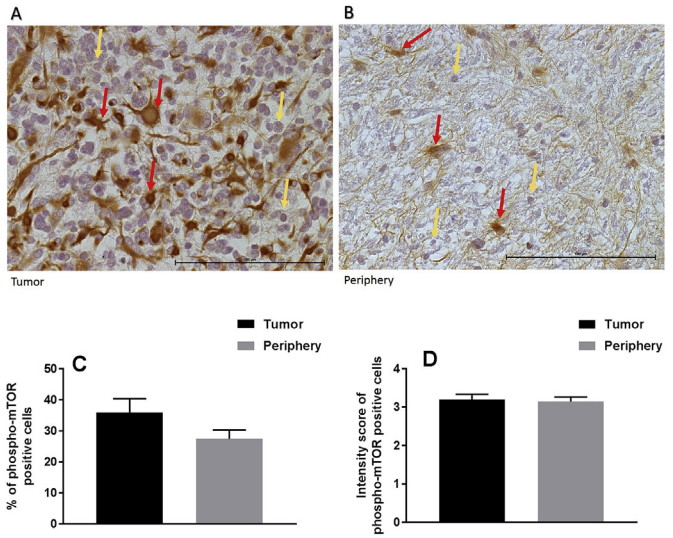

Fig. 1. Evaluation of mTOR pathway in GBM specimens. Panel A shows a representative image of phospho-mTOR staining in GBM sample (magnitude 40x), Panel B shows a representative image of phospho-mTOR staining in periphery around the tumor (magnitude 40x). Red arrow shows positive cells; yellow arrow shows negative cells. Panel C shows the percentage of cells expressing phospho-mTOR, whereas panel D shows the average of intensity score of phospho-mTOR positive cells.

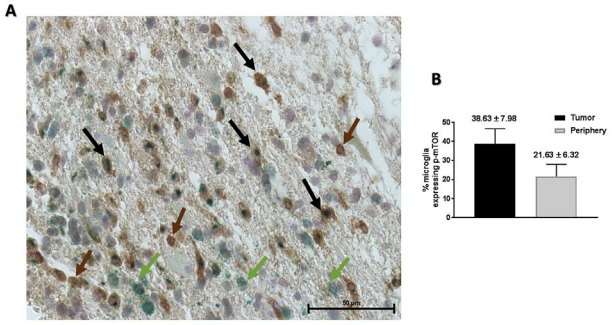

Fig. 2. Evaluation of microglia-macrophages expressing phospho-mTOR. Panel A shows a representative image of phospho-mTOR and IBA1 double staining in glioma specimens. Brown arrow shows IBA1 positive cells, green arrow shows phospho-mTOR positive cells, and black arrow shows phospho-mTOR and IBA1 positive cells. Panel B shows the percent of microglia-macrophage phospho-mTOR + expressing in GBM specimens (black box) and in periphery (grey box).

pre-stimulated conditioned medium (PS-CM).

To characterize the CMs, we measured levels of end-products of the above genes, namely IL1β, IL-6, PGE2, urea and NO, in the incubation medium. We found that NO (expressed as nitrite levels) was undetectable in either B-CMs or PS-CMs obtained from either U87MG or T98G cells (not shown). In contrast, significant urea levels could be detected at baseline both in T98G CMs (1 μg/ml on average) and in U87MG CMs (3 μg/ml on average), but those levels were not different when the U87MG or T98G were pre-stimulated with the mixture of cytokines (data not shown). We observed significant 1.5-fold, 4-fold and 5-fold increases in PGE2, IL6 and IL1β levels, respectively, in U87MG PS-CM compared to B-CMs (Fig. 4). In T98G PS-CM we also found a 3-fold and 6-fold increase in IL1 β and IL6 levels, respectively, as compared to B-CMs, whereas no change was observed in PGE2 levels (Fig. 4).

3.3. Effects of B-CM and PS-CM obtained from glioma cell lines on human microglia CHME-5 cells

We next conducted a series of experiments in which the human microglia CHME-5 cells were exposed to CMs. Cells were incubated with graded concentrations of CMs (i.e. 25% CM + 75% plain medium, 50% CM + 50% plain medium, 100% CM) over a period of 0–72 h (Fig. 5). CHME-5 cell growth in plain medium reached a peak within 16–24 h, and remained stable up to up to 48 h; thereafter, an increase in the number of dead cells was observed (Fig. 5A). This growth profile remained unchanged when the percent of CMs in the media was increased, with 2 exceptions: at all times tested, 100% B-CM from U87MG, but not T98G cells increased the total number of live cells, whereas an increase in lethality was observed after exposure to 100% PS-CM from T98G cells (Fig. 5B–C). We found no dose-dependent effect of CM on cell growth; however, a dose-dependent effect was observed on lethality induced by PS-CM from T98G cells (not shown). Because of the increase in lethality observed after 48 h of incubation, all subsequent experiments were carried out between 0 and 48 h.

To investigate the phenotypic profile induced in CHME-5 cells by the different CMs, we measured levels of urea and NO released in the medium, as markers of L-arginine metabolism through the ARG/NOS pathways, as well as expression of TNFα, iNOS, TGFβ and IL10 mRNAs. We found that both B-CM and PS-CM elicited dose-dependent increases in urea levels, which reached statistical significance compared to plain medium from 50% of CMs from T98G cells, and at 100% of CMs from U87MG cells (Fig. 6). On the contrary, we found no difference in NO levels compared to controls, nor any change in iNOS mRNA levels, or in any of the other genes tested (not shown).

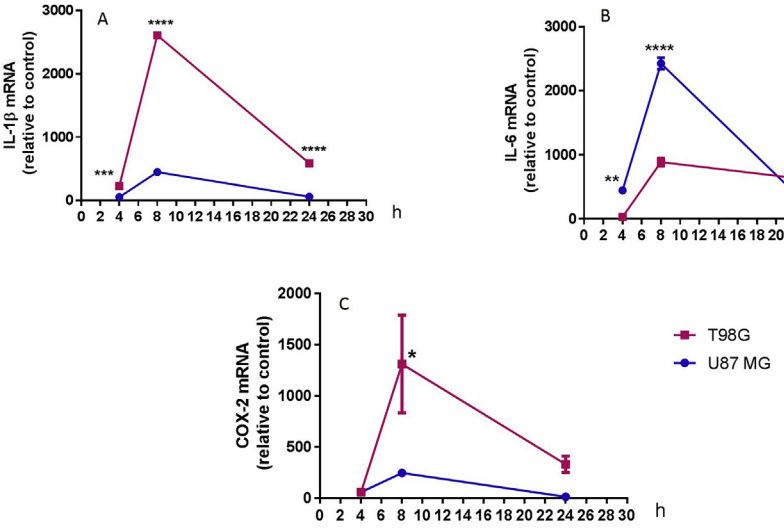

Fig. 3. Evaluation of pro-inflammatory gene expression elicited by cytokines in glioma cell lines. Panel A, B and C show time-dependent up-regulation of IL-1β, IL-6 and COX2 gene expression respectively in U87MG (blue line) and in T98G (red line). *,**,***,****p < 0,05, p < 0,01, p < 0,001 or p < 0,0001 respectively T98G vs U87MG in each time point. Two-way ANOVA analysis was carried out.

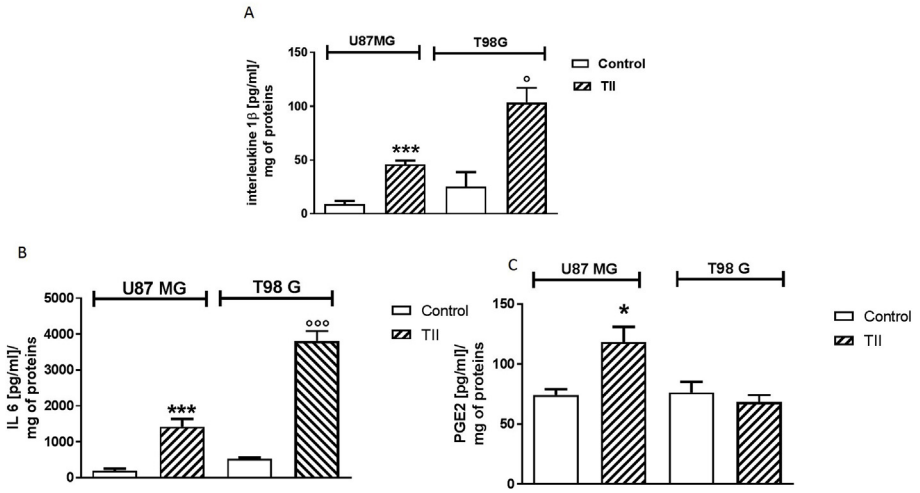

Fig. 4. Evaluation of pro-inflammatory products in CM obtained after pre-stimulation with cytokines challenge. Panel A, B and C show the level of IL-1β, IL-6 and PGE2. *, ***p < 0,05 or p < 0,001 respectively vs U87 MG control or °, °°°p < 0,05 or p < 0,001 respectively vs T98 G control. Student's *t*-test was carried out (basal *vs* pre-stimulated).

Moreover, we sought to investigate the effects of CMs on CHME-5 cells that were previously stimulated with TII for 4 h; indeed, such pre-stimulation drives CHME-5 cells into an activated M1 profile (Lisi et al., 2017b). Under these conditions, we found significant change in urea levels elicited by T98G CMs (Fig. 7), however by comparing the urea releases promoted by all CMs into not pre-stimulated cells (or pre-treated with medium) versus cells pre-treated with TII, all CMs significantly increase urea releases (Fig. 7). In contrast to non-prestimulated cells, all CMs significantly increased iNOS mRNA levels in CHME-5 cells that were prestimulated with TII for 4 h (Fig. 8). The iNOS mRNA levels were increased after 4 h stimulation with CMs, but after longer exposure times (i.e. 24 or 48 h), increases were no longer observed. After 48 h incubation, the NO levels were increased by pre-treatment with TII (Fig. 8C), but were consistently reduced by the presence of any CMs. Taken together the data suggest that CMs induce a M2 profile in both resting microglia (Fig. 6) and in pre-stimulated M1 microglia (Figs. 7 and 8), although in the latter with a transient response.

3.4. Involvement of mTOR pathway in glioma-microglia interaction

We next tested if the mTOR pathway is activated in human microglia after exposure to human glioma-derived CMs. We found that both T98G B-CM and PS-CMs, but not U87MG CMs, significantly increased phosphorylation of mTOR at Ser2448 with respect to controls after 2-h incubation periods (Fig. 9A). In parallel, mTOR downstream factor 4EBP1 was significantly modified by B-CMs (Fig. 9B). Similarly, another mTOR downstream factor, p-P70S6k was significantly increased in the presence of all CMs (Fig. 9C). We also looked at the mechanisms of mTOR activation; interestingly, the upstream factor TSC2 was significantly decreased in the presence of CMs (Fig. 10).

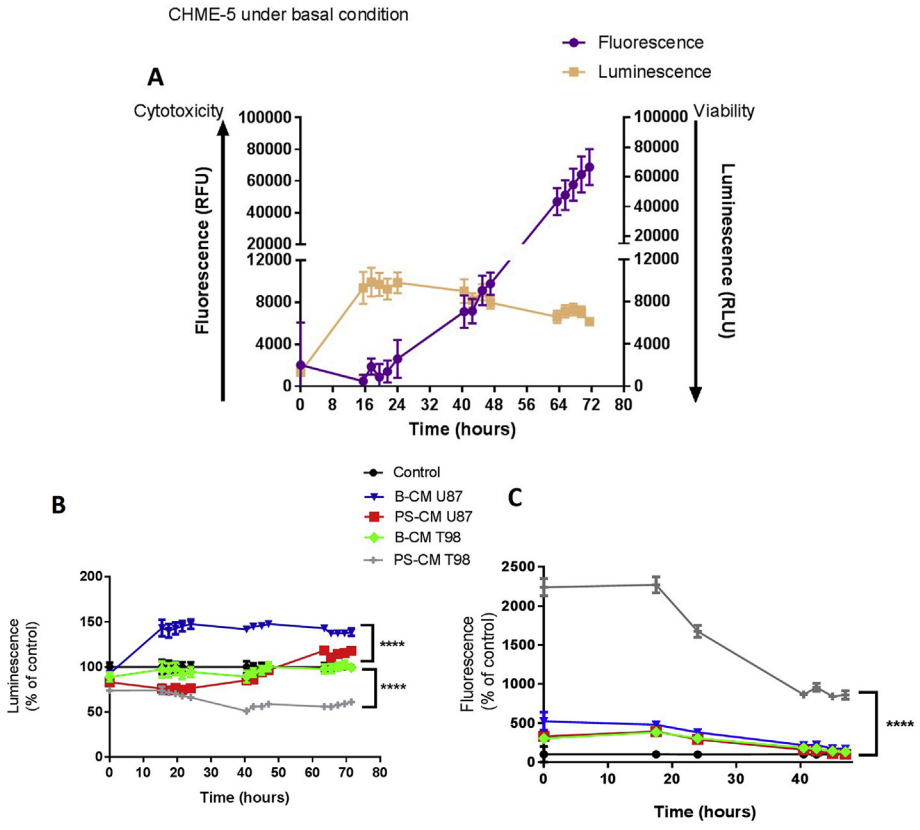

Fig. 5. Evaluation of cell viability and cell mortality of CHME-5 Cells. Panel A shows the growth of CHME-5 cell line (20.000 cells/well) under basal conditions in plain growth media. The fluorescence data indicates the not viability cells whereas the luminescence data indicates the viability cells. Panel B and C show the cell viability and cell mortality respectively in the presence of the indicated CMs. For each time point the data are expressed relative to the control, which is taken as 100%. ****p < 0,0001 CM vs basal condition. Two-way ANOVA analysis was carried out.

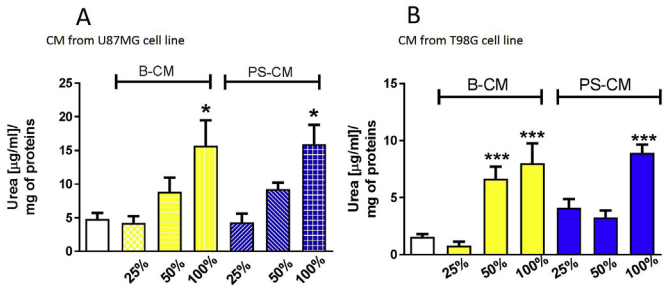

Fig. 6. Effects of CMs on urea release. Left panel shows the urea content in CHME-5 cells, under basal condition (white), after U87MG B-CM challenge (yellow) and after U87MG PS-CM stimulation (blue). Right panel shows the urea content in CHME-5 cells, under basal condition (white), after T98G B-CM challenge (yellow) and after T98G PS-CM stimulation (blue). The data are obtained after 48 h of incubation. *, ***p < 0,05 or p < 0,001 respectively vs control. One-way ANOVA analysis was carried out.

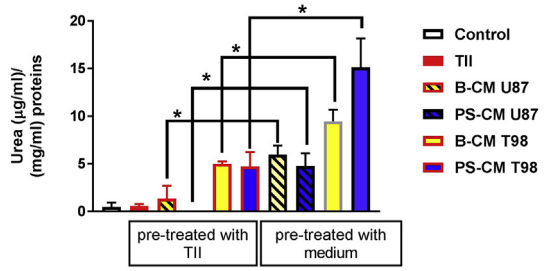

Fig. 7. Effects of CMs on M1 CHME-5. CHME-5 were pre-stimulated with TII for 4 h. After 4 h cytokines were removed, CMs were administrated for the subsequent 48 h and urea content were measured. As indicated in figure boxes 2-3-4-5-6 were pre-treated with TII, boxes 7-8-9-10 were pre-treated with medium. *p < 0,05 vs TII CMs. One-way ANOVA analysis followed by Bonferroni's post-test was carried out.

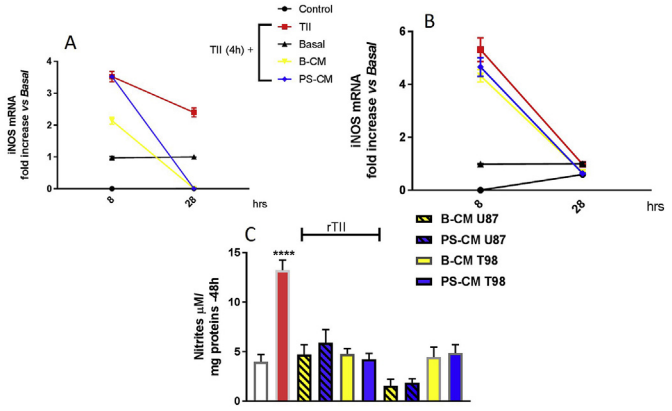

Fig. 8. Evaluation of iNOS pathway after CMs challenge. CHME-5 were pre-stimulated with TII for 4 h. After 4 h cytokines were removed, CMs were administrated for the subsequent 4 or 24 h and iNOS gene expression were measured. Panel A show the effects of U87MG CMs on iNOS gene expression in CHME-5. Panel B show the effects of T98G CMs on iNOS gene expression in CHME-5. Panel C shows nitrite content in 48-h experiments in CHME-5. White bar indicates the control group whereas the red bar the TII group. ***p < 0,001 vs control. One-way ANOVA analysis followed by Bonferroni's post-test was carried out.

3.5. Effects of mTOR inhibitors on the glioma-microglia paradigm

Under basal conditions, CHME-5 cells express high levels of Raptor A (major component of mTORC1) and Rictor (a major component of mTORC2) gene expression. None of the CMs used -regardless of cell origin or pre-stimulation state-effected that gene expression (data not shown), nor did incubation with the mTOR inhibitor RAPA modify either Raptor and Rictor gene expression in the presence of any of the CMs (data not shown).

Despite absence of effects on mTOR components, RAPA (10–100 nM) decreased urea production (Fig. 11) and ARG1 expression (Fig. 12) from CHME-5 cells exposed to B-CMs or PS-CMs. In addition, incubation with RAPA had no effects on either IL6, ARG1, or IL10 gene expression. RAPA increased gene expression of iNOS 4-fold versus iNOS levels due to the presence of CMs only (data not shown); however that increase was not associated with any increase in NO levels at 48 h. These data are consistent with our previous observations in the rat model (Lisi et al., 2014a), and reinforce the idea that the blockade of mTOR is associated with a modification of M2/M1 ratio.

4. Discussion

In the present study, we used two different approaches (i.e. human tumor specimens and human cell models) to study the activation of the mTOR pathway in glioma-associated microglia. In particular, by immunostaining analysis of surgical GBM specimens from 42 patients, we showed phosphorylated-mTOR expression and localization in microglia-macrophage cells. In addition, these findings were confirmed in functional experiments. Using U87MG or T98G cells as a model for human glioma and CHME-5 cells to model human microglia, we investigated the involvement of mTOR in *in vitro* paradigms of microglia-glioma interaction under two different conditions (Figure Suppl 1).

In the last decade, the role of microglia in GBM pathology is becoming clearer. Under the influence of GBM, microglia tend to assume a M2 phenotype, which has predominantly a pro-tumor role. However, in addition to this role, evidence that is more recent indicates that some cells with microglial characteristics seen in GBMs are actually part of the tumor cell population. According to these findings, the expression of CD163, an M2 microglia marker, is also a marker for fusion hybrids between immune cells (macrophages or microglia) and neoplastic tumor cells (Huysentruyt et al., 2011; Lindström et al., 2017; Gast et al., 2018). In this context, we recently found that in surgical GBM specimens CD163 expression is higher within GBM specimens than in the surrounding periphery in both male and female patients. (Lisi et al., 2017a). Taken together these findings lead to the hypothesis that under specific conditions microglial cells may lose characteristics of the immune system and acquire tumor-cell characteristics. However, additional studies are required to confirm or negate these possibilities.

In our studies, we used production of urea to serve as an index of arginine metabolism (an M2 type phenotype). The main source of urea in eukaryotes is from conversion of arginine to ornithine by the enzyme arginase. However, urea can also be generated from glutamine via action of glutaminase which produces ammonia which can then be condensed with CO2 to generate urea (Bach and Smith, 1956); a process which mainly occurs in liver. However, most glial derived tumor cells depend upon glutamine for growth (Szeliga et al., 2009; Szeliga and Albrecht, 2016), associated with expression of a phosphate activated glutaminase (Majewska et al., 2017) to generate glutamate as an energy source. It is therefore possibly that treatments of T98G (and U87MG) cells that modify urea production may be due in part to changes in phosphate activated glutaminase. Moreover, the suppression of urea release due to mTOR inhibitors could be due to reductions in glutaminase expression, which could contribute to the ability of these inhibitors to reduce glioma growth. This would be consistent with findings that up-regulation of glutaminase in certain glioblastoma cell lines renders them resistant to mTOR inhibition (Tanaka et al., 2015).

Using the human microglia-glioma interaction paradigm, we showed that the mTOR pathway is fully activated in microglia cells under conditions mimicking the human GBM pathology. Such mTOR activation, observed as increases in phosphorylated mTOR fraction, is in full agreement with data from human tumor specimens, showing that

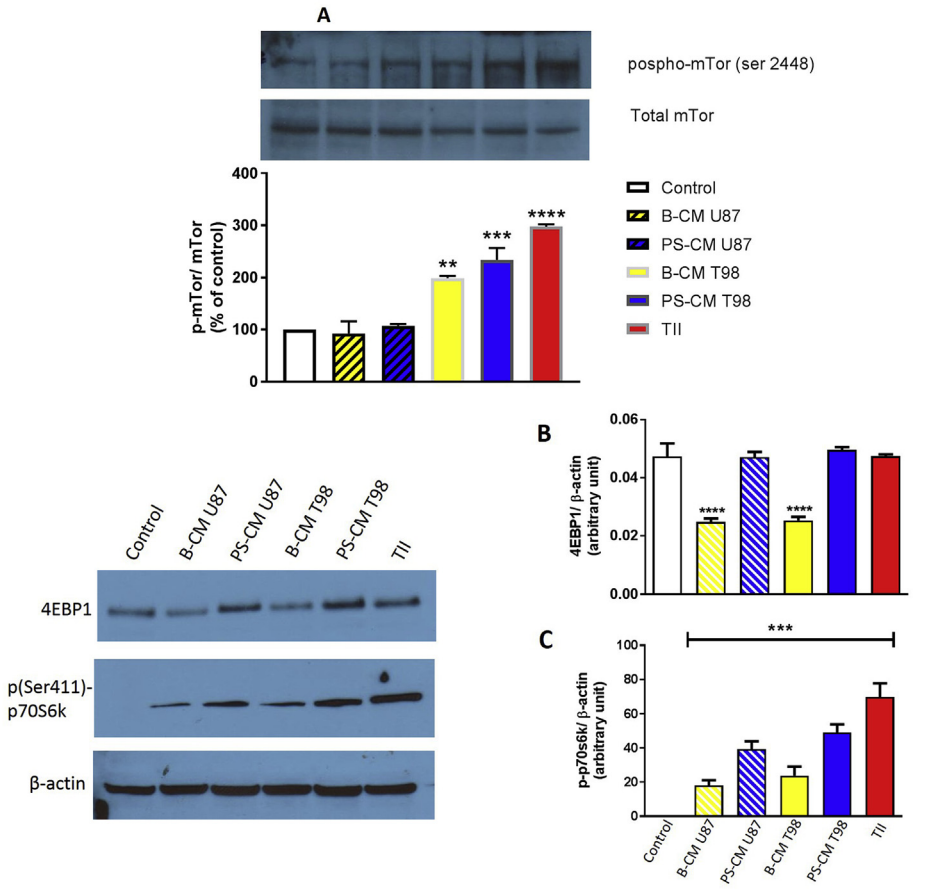

Fig. 9. Evaluation of mTOR pathway in *in vitro* microglia-glioma interaction. Western blot analysis of CHME-5 lysates prepared 2 h after the following treatments: Lane 1, control, 2, U87MG B-CM; 3, U87MG PS-CM; 4, T98G B-CM; 5, T98G PS-CM; 6, TII. Panel A shows western blot analysis for phospho-mTOR Serine 2448 (top image) and total mTOR (bottom image), panel B shows 4EBP1 quantification and panel C shows p-P70S6K quantification. *, **, ***p < 0,05 p < 0,01 or p < 0,001 respectively vs control. One-way ANOVA analysis followed by Bonferroni's post-test was carried out.

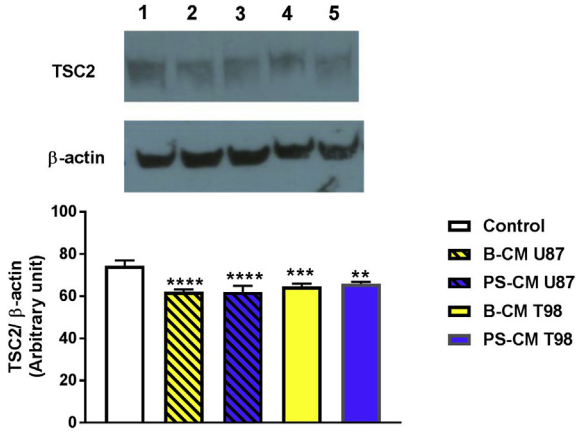

Fig. 10. Evaluation of TSC2 in *in vitro* microglia-glioma interaction. Western blot analysis of CHME-5 lysates for TSC2 (top image) and β-actin (bottom image) prepared 2 h after the following treatments: Lane 1, control; 2, U87MG B-CM; 3, U87MG PS-CM; 4, T98G B-CM; 5, T98G PS-CM. **, ***,****p < 0,01, p < 0,001 or p < 0,0001 respectively vs control. One-way ANOVA analysis followed by Bonferroni's post-test was carried out.

39% of microglia-macrophage in glioma specimens express mTOR phosphorylated at Ser-2448, taken as marker of mTORC1 activation (Rosner et al., 2010). In addition, and consistent with previous data from our group and others, here we show that microglia express an M2 pro-tumor phenotype in the presence of glioma cells, and that this M2 phenotype is down-regulated in the presence of an mTOR inhibitor. Based on the above data, we hypothesize that the blockade of mTOR in GBM patients might induce a reduction in M2 phenotype expression in about 40% of all tumor-associated microglia. In this regard, it is important to emphasize that microglia may represent 30–70% of the entire tumor (Wood GW and Morantz, 1979; Roggendorf et al., 1996; da Fonseca and Badie, 2013).

In the present study, we reported data using two different glioma cell lines. Preliminary data (Figs. 3 and 4) showed that conditioned media obtained by U87MG or T98G are similar but not identical in term of IL6, IL1β and PGE2 release. In fact, CMs obtained from T98G contain more IL6 and IL1β than that from U87MG but contain less PGE2. These differences could explain why in some conditions (i.e phospho-mTOR activation) CMs give different results.

Here we showed that mTOR activation could be elicited through different pathways, depending on different experimental conditions. In fact, when CHME-5 cells were treated with B-CM [a condition mimicking an early stage of pathology (Lisi et al., 2014b)], the activation of mTOR pathway was associated with a significant blockade of TSC2. On the contrary, when CHME-5 cells were exposed to PS-CM [a condition that mimics a late stage of pathology (Lisi et al., 2014b)], mTOR activation was in part independent from TSC2 inactivation. While TSC2 inhibition is considered as the 'classical' pathway of TOR activation, TSC2-independent mechanisms have also been described. Upstream oncogenic mutations activate mTORC1 kinase via at least two alternative mechanisms: down-regulation/inactivation of TSC2 and phosphorylation of the mTORC1 inhibitor PRAS40 by AKT (Huang and Manning, 2009; Lv et al., 2017). The TSC2 protein integrates signals from three pathways (AKT, ERK/RSK, and LKB1/AMPK); each of these pathways can lead to phosphorylation of several serines and threonines on TSC2. The latter in turn acts as a GTPase-activating protein for the small Ras-like protein, Rheb. Whereas Rheb bound to GDP is thought to be inactive, Rheb-GTP is an essential activator for mTORC1 kinase (Dibble and Cantley, 2015). Phosphorylation of PRAS40 by AKT inhibits the binding of PRAS40 to mTORC1 and the subsequent mTORC1 kinase activation (Lv et al., 2017).

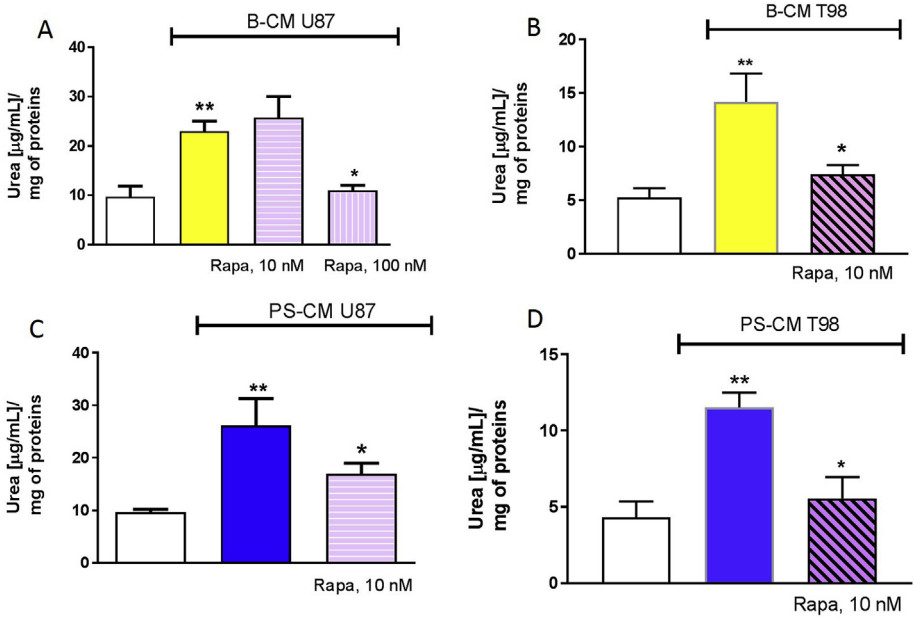

Fig. 11. Effects of rapamycin on urea levels in CHME-5 after stimulation with CMs (48 h experiments). **p < 0,01 vs control; ° p < 0,05 vs CM. One-way ANOVA analysis followed by Bonferroni's post-test was carried out.

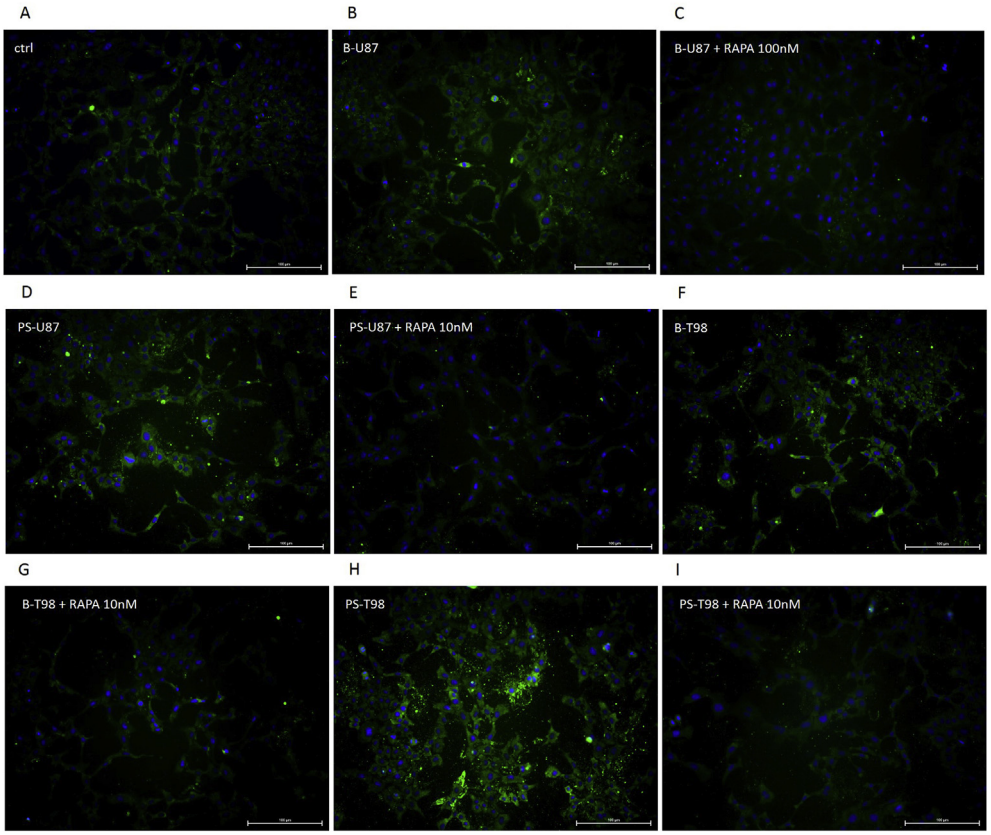

Fig. 12. Effects of rapamycin on ARG1 expression in CHME-5 after stimulation with CMs (24 h experiments). Panel A, control; B, B-CM; C, B-CM + Rapa 100 nM; D, PS-U87; E, PS-U87 + Rapa 10 nM; F, B-T98; G, B-T98 + Rapa 10 nM; H, PS-T98; I, Ps-T98 + Rapa 10 nM.

Because of their availability as immunosuppressive agents, mTOR inhibitors have been extensively investigated in clinical trials in oncology, based on their ability to control cell proliferation. So far, the efficacy of everolimus (RAD0001) has been demonstrated as a second line treatment in renal, breast and neuroendocrine cancers of lung, pancreatic or gastrointestinal origin. Overall, mTOR inhibitors have had limited success in clinical trials for various other tumor types (in glioma but also in major solid tumors). The reasons for such limited success are yet to be clarified, but may be related to the inhibition of a large number of mTORC1-regulated signaling systems normally involved in tumor suppression, such as the activation of receptor tyrosine kinases (RTKs), PI3K-Akt signaling, and Ras-ERK pathway (Nussinov

et al., 2018). In order to overcome these limitations, alternative strategies have been explored in the past few years and a number of ATP-competitive mTOR inhibitors have been developed, which block both mTORC1 and mTORC2 activity. Unlike RAPA, which is a specific allosteric inhibitor of mTORC1, these ATP-competitive inhibitors target the catalytic site of the enzyme, thus promoting a broader, more potent and sustained inhibition of mTOR, thereby preventing the activation of PI3K/Akt caused by the de-repression of negative feedbacks (Martelli et al., 2018). In addition, it is important to consider that glucose and glutamine are drivers of mTOR activation (Tanaka et al., 2015) and in particular, glucose drives GBM through the PI3K-AKT pathway (Shukla et al., 2018). Therefore another possible way to escape the limited success of mTOR inhibitor in clinical trials could be use therapies that target glucose and glutamine to affect the mTOR pathway. However, while the inhibition of mTOR pathway remains a meaningful target for the treatment of GBM, novel and more specific molecules are needed.

In conclusion, a main finding of this study the observation that the mTOR pathway is activated in 39% of microglia-macrophage within GBM tumors, compared to 21% in peripheral tissues. We also showed that pharmacological inhibition of mTOR reduce urea levels and ARG1 expression -taken as a M2 marker-in *in vitro* models of both early- and late stage glioma. Since the M2 profile of microglial activation is widely thought to be associated to tumor progression (Annovazzi et al., 2018), the increase in the ratio of M1 microglia bearing cytotoxic and anti-tumor activity brought about by mTOR inhibition might be envisioned as an additional antitumor mechanism of mTOR inhibitors, along with direct anti-proliferative activity.

Author contribution

Study concepts: LL; PN.
Study design: LL; AM.
Data acquisition: GMPC; MC; MP; SK.
Data analysis and interpretation: LL; SK; DLF.
Statistical analysis: LL; DLF; PN.
Manuscript preparation: LL.
Manuscript editing: PN.
Manuscript review: AM, DLF and PN.

Funding

Fondi Ateneo 2017 (PN) financed the research.

Conflict of interest

Any conflicts of interest to disclose.

Appendix A. Supplementary data

Supplementary data to this article can be found online at https://doi.org/10.1016/j.neuint.2019.104485.

References

Amin, S.A., Adhikari, N., Baidya, S.K., Gayen, S., Jha, T., 2018. Structural refinement and prediction of potential CCR2 antagonists through validated multi-QSAR modeling studies. J. Biomol. Struct. Dyn. 3, 1–20. https://doi.org/10.1080/07391102.2017.1418679.

Annovazzi, L., Mellai, M., Bovio, E., Mazzetti, S., Pollo, B., Schiffer, D., 2018. Microglia immunophenotyping in gliomas. Oncol. Lett. 15 (1), 998–1006. https://doi.org/10.3892/ol.2017.7386.

Arbab, A.S., Rashid, M.H., Angara, K., Borin, T.F., Lin, P.C., Jain, M., Achyut, B.R., 2017. Major challenges and potential microenvironment-targeted therapies in glioblastoma. Int. J. Mol. Sci. 18 (12) pii, E2732. https://doi.org/10.3390/ijms18122732.

Atzori, M.G., Tentori, L., Ruffini, F., Ceci, C., Lisi, L., Bonanno, E., Scimeca, M., Eskilsson, E., Daubon, T., Miletic, H., Ricci Vitiani, L., Pallini, R., Navarra, P., Bjerkvig, R., D'Atri, S., Lacal, P.M., Graziani, G., 2017. The anti-vascular endothelial growth factor receptor-1 monoclonal antibody D16F7 inhibits invasiveness of human glioblastoma and glioblastoma stem cells. J. Exp. Clin. Cancer Res. 36 (1), 106. https://doi.org/10.1186/s13046-017-0577-2.

Bach, S.J., Smith, M., 1956. Glutamine; a nitrogen source in urea synthesis. Biochem. J. 64 (3), 417–425.

Chen, Z., Hambardzumyan, D., 2018. Immune microenvironment in glioblastoma subtypes. Front. Immunol. 8 (9), 1004. https://doi.org/10.3389/fimmu.2018.01004.

da Fonseca, A.C., Badie, B., 2013. Microglia and macrophages in malignant gliomas: recent discoveries and implications for promising therapies. Clin. Dev. Immunol. 2013, 264124. https://doi.org/10.1155/2013/264124.

Dello Russo, C., Lisi, L., Tentori, L., Navarra, P., Graziani, G., Combs, C.K., 2017. Exploiting microglial functions for the treatment of glioblastoma. Curr. Cancer Drug Targets 17 (3), 267–281. https://doi.org/10.2174/1568009616666160813191240.

Dello Russo, C., Lisi, L., Tringali, G., Navarra, P., 2009. Involvement of mTOR kinase in cytokine-dependent microglial activation and cell proliferation. Biochem. Pharmacol. 78 (9), 1242–1251. https://doi.org/10.1016/j.bcp.2009.06.097.

Dibble, C.C., Cantley, L.C., 2015. Regulation of mTORC1 by PI3K signaling. Trends Cell Biol. 25 (9), 545–555. https://doi.org/10.1016/j.tcb.2015.06.002.

Foster, K.G., Fingar, D.C., 2010. Mammalian target of rapamycin (mTOR): conducting the cellular signaling symphony. J. Biol. Chem. 285 (19), 14071–14077. https://doi.org/10.1074/jbc.R109.094003.

Gast, C.E., Silk, A.D., Zarour, L., Riegler, L., Burkhart, J.G., Gustafson, K.T., Parappilly, M.S., Roh-Johnson, M., Goodman, J.R., Olson, B., Schmidt, M., Swain, J.R., Davies, P.S., Shasthri, V., Iizuka, S., Flynn, P., Watson, S., Korkola, J., Courtneidge, S.A., Fischer, J.M., Jaboin, J., Billingsley, K.G., Lopez, C.D., Burchard, J., Gray, J., Coussens, L.M., Sheppard, B.C., Wong, M.H., 2018. Cell fusion potentiates tumor heterogeneity and reveals circulating hybrid cells that correlate with stage and survival. Sci. Adv. 4 (9) eaat7828. https://doi.org/10.1126/sciadv.aat7828.

Huang, J., Manning, B.D., 2009. A complex interplay between Akt, TSC2 and the two mTOR complexes. Biochem. Soc. Trans. 37 (Pt 1), 217–222. https://doi.org/10.1042/BST0370217.

Huysentruyt, L.C., Akgoc, Z., Seyfried, T.N., 2011. Hypothesis: are neoplastic macrophages/microglia present in glioblastoma multiforme? ASN Neuro. 22 (4), 3. https://doi.org/10.1042/AN20110011.

Janabi, N., Peudenier, S., Héron, B., Ng, K.H., Tardieu, M., 1995. Establishment of human microglial cell lines after transfection of primary cultures of embryonic microglial cells with the SV40 large T antigen. Neurosci. Lett. 195 (2), 105–108. https://doi.org/10.1016/0304-3940(94)11792-H.

Liang, F., Giordano, C., Shang, D., Li, Q., Petrof, B.J., 2018. The dual CCR2/CCR5 chemokine receptor antagonist Cenicriviroc reduces macrophage infiltration and disease severity in Duchenne muscular dystrophy (Dmdmdx-4Cv) mice. PLoS One 13 (3), e0194421. https://doi.org/10.1371/journal.pone.0194421.

Lindström, A., Midtbö, K., Arnesson, L.G., Garvin, S., Shabo, I., 2017. Fusion between M2-macrophages and cancer cells results in a subpopulation of radioresistant cells with enhanced DNA-repair capacity. Oncotarget 8 (31), 51370–51386. https://doi.org/10.18632/oncotarget.17986.

Lisi, L., Ciotti, G.M., Braun, D., Kalinin, S., Currò, D., Dello Russo, C., Coli, A., Mangiola, A., Anile, C., Feinstein, D.L., Navarra, P., 2017. Expression of iNOS, CD163 and ARG-1 taken as M1 and M2 markers of microglial polarization in human glioblastoma and the surrounding normal parenchyma. Neurosci. Lett. 645, 106–112. https://doi.org/10.1016/j.neulet.2017.02.076.

Lisi, L., Laudati, E., Navarra, P., Dello Russo, C., 2014b. The mTOR kinase inhibitors polarize glioma-activated microglia to express a M1 phenotype. J. Neuroinflammation 11, 125. https://doi.org/10.1186/1742-2094-11-125.

Lisi, L., Navarra, P., Feinstein, D.L., Dello Russo, C., 2011. The mTOR kinase inhibitor rapamycin decreases iNOS mRNA stability in astrocytes. J. Neuroinflammation 8 (1), 1. https://doi.org/10.1186/1742-2094-8-1.

Lisi, L., Pizzoferrato, M., Miscioscia, F.T., Topai, A., Navarra, P., 2017b. Interactions between integrase inhibitors and human arginase 1. J. Neurochem. 142 (1), 153–159. https://doi.org/10.1111/jnc.14039.

Lisi, L., Stigliano, E., Lauriola, L., Navarra, P., Dello Russo, C., 2014. Proinflammatory-activated glioma cells induce a switch in microglial polarization and activation status, from a predominant M2b phenotype to a mixture of M1 and M2a/B polarized cells. ASN Neuro. 6 (3), 171–183. https://doi.org/10.1042/AN20130045.

Lu, V.M., Jue, T.R., McDonald, K.L., Rovin, R.A., 2018. The survival effect of repeat surgery at glioblastoma recurrence and its trend: a systematic review and meta-analysis. World Neurosurg. 115, 453–459. e3. https://doi.org/10.1016/j.wneu.2018.04.016.

Lv, D., Guo, L., Zhang, T., Huang, L., 2017. PRAS40 signaling in tumor. Oncotarget 8 (40), 69076–69085. https://doi.org/10.18632/oncotarget.17299.

Majewska, E., Rola, R., Barczewska, M., Marquez, J., Albrecht, J., Szeliga, M., 2017. Transcription factor GATA3 expression is induced by GLS2 overexpression in a glioblastoma cell line but is GLS2-independent in patient-derived glioblastoma. J. Physiol. Pharmacol. 68 (2), 209–214.

Martelli, A.M., Buontempo, F., McCubrey, J.A., 2018. Drug discovery targeting the mTOR pathway. Clin. Sci. 132 (5), 543–568. https://doi.org/10.1042/CS20171158.

Miyauchi, J.T., Tsirka, S.E., 2018. Advances in immunotherapeutic research for glioma therapy. J. Neurol. 265 (4), 741–756. https://doi.org/10.1007/s00415-017-8695-5.

Nussinov, R., Tsai, C.J., Jang, H., 2018. Oncogenic Ras isoforms signaling specificity at the membrane. Cancer Res. 78 (3), 593–602. https://doi.org/10.1158/0008-5472.CAN-17-2727.

Roggendorf, W., Strupp, S., Paulus, W., 1996. Distribution and characterization of microglia/macrophages in human brain tumors. Acta Neuropathol. 92 (3), 288–293. https://doi.org/10.1007/s004010050520.

Rosner, M., Siegel, N., Valli, A., Fuchs, C., Hengstschlager, M., 2010. mTOR phosphorylated at S2448 binds to raptor and rictor. Amino Acids 38 (1), 223–228. https://doi.org/10.1007/s00726-008-0230-7.

Shukla, A., Gupta, P., Singh, R., Mishra, D.P., 2018. Glycolytic inhibitor 2-Deoxy-d-

Glucose activates migration and invasion in glioblastoma cells through modulation of the miR-7-5p/TFF3 signaling pathway. Biochem. Biophys. Res. Commun. 499 (4), 829–835. https://doi.org/10.1016/j.bbrc.2018.04.001.

Szeliga, M., Albrecht, J., 2016. Glutamine metabolism in gliomas. Adv. Neurobiol. 13, 259–273. https://doi.org/10.1007/978-3-319-45096-4_9.

Szeliga, M., Obara-Michlewska, M., Matyja, E., Łazarczyk, M., Lobo, C., Hilgier, W., Alonso, F.J., Márquez, J., Albrecht, J., 2009. Transfection with liver-type glutaminase cDNA alters gene expression and reduces survival, migration and proliferation of T98G glioma cells. Glia 57 (9), 1014–1023. https://doi.org/10.1002/glia.20825.

Tanaka, K., Sasayama, T., Irino, Y., Takata, K., Nagashima, H., Satoh, N., Kyotani, K., Mizowaki, T., Imahori, T., Ejima, Y., Masui, K., Gini, B., Yang, H., Hosoda, K., Sasaki, R., Mischel, P.S., Kohmura, E., 2015. Compensatory glutamine metabolism promotes glioblastoma resistance to mTOR inhibitor treatment. J. Clin. Investig. 125 (4), 1591–1602. https://doi.org/10.1172/JCI78239.

Tee, A.R., 2018. The target of rapamycin and mechanisms of cell growth. Int. J. Mol. Sci. 19 (3) pii: E880. https://doi.org/10.3390/ijms19030880.

Tsutsumi-Kuroda, U., Inoue, T., Futakuchi, A., Shobayashi, K., Takahashi, E., Kojima, S., Inoue-Mochita, M., Fujimoto, T., Tanihara, H., 2018. Decreased MCP-1/CCR2 axis-mediated chemotactic effect of conjunctival fibroblasts after transdifferentiation into myofibroblasts. Exp. Eye Res. 170, 76–80. https://doi.org/10.1016/j.exer.2018.02.008.

Weller, M., 2018. Next generation neuro-oncology. Eur. J. Cancer 96, 1–5. https://doi.org/10.1016/j.ejca.2018.03.016.

Wood, G.W., Morantz, R.A., 1979. Immunohistologic evaluation of the lymphoreticular infiltrate of human central nervous system tumors. J. Natl. Cancer Inst. 62 (3), 485–491.